

Quantification of a PbCl_x Shell on the Surface of PbS Nanocrystals

Samuel W. Winslow,[†] Yun Liu,^{‡,¶} James W. Swan,^{*,†} and William A. Tisdale^{*,†}

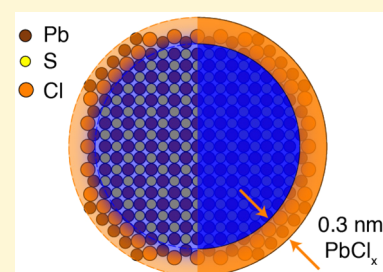
[†]Department of Chemical Engineering, Massachusetts Institute of Technology, Cambridge, Massachusetts 02142, United States

[‡]Center for Neutron Research, National Institute of Standards and Technology, Gaithersburg, Maryland 20899, United States

[¶]Department of Chemical and Biomolecular Engineering, University of Delaware, Newark, Delaware 19716, United States

Supporting Information

ABSTRACT: Differences between the properties of PbS nanocrystals prepared using a large excess of PbCl_2 and those prepared using other Pb sources have led to speculation that a thin PbCl_x shell may be present on the surface of PbCl_2 -derived PbS nanocrystals. However, characterization of this chloride layer has proven to be challenging because of the poor contrast provided by electron and X-ray scattering probes. Here, we show that small-angle neutron scattering (SANS) provides the compositional sensitivity needed to unambiguously quantify the PbCl_x shell that is present on the surface of PbCl_2 -derived PbS nanocrystals. Using a charge-balanced structural model, the scattering contribution of a ~ 0.3 nm thick surface PbCl_x layer is parsed separately from ligand carboxylate head groups and PbS in the core. Global fitting of the SANS data across a solvent deuteration series enables unique determination of the spatial distribution of each material. These results are corroborated by quantitative nuclear magnetic resonance (NMR) and energy-dispersive X-ray spectroscopy (EDS). This work resolves a discrepancy in reported sizing curves for PbS nanocrystals prepared by different syntheses and further demonstrates the power of SANS in resolving molecular structure in soft and hybrid nanomaterials.



PbS quantum dots (QDs) have been investigated as the active material in many next-generation optoelectronic devices.¹ The broadly tunable absorbance/emission across the near-infrared spectrum makes PbS particularly exciting for use in photodetector and photovoltaic technologies.^{2–7} At the nanoscale, the high surface-to-volume ratio in these materials means the surface structure and energetics are critical to determining ensemble properties. Indeed, the core surface has a profound effect on energy-level modification⁸ and electron-phonon coupling.^{9,10}

There are multiple synthetic routes for producing PbS QDs using either PbO ¹¹ or PbCl_2 ¹² as the lead precursors. However, there are notable differences in the reported materials from each synthesis. A sizing curve for PbO -based PbS QDs¹³ yields smaller nanocrystal sizes for a given first exciton absorption peak as compared to a sizing curve for PbS QDs synthesized with a large excess of PbCl_2 .¹⁴ Additionally, the reported Pb/S ratio in PbCl_2 -based QDs is higher than that for PbO -based QDs, and residual Cl can be detected even after washing.¹⁴

Circumstantial evidence suggests that PbS QDs prepared from a PbCl_2 precursor may be coated with an insulating PbCl_x shell.^{15,16} Additional anecdotal evidence supporting the presence of an insulating PbCl_x shell includes (1) improved resistance of chloride-based PbS QDs to oxidation and prolonged stability,^{14,15,17} (2) slower charge carrier hopping times for lead halide based lead chalcogenide QDs,^{18–21} and (3) superior triplet sensitization capability of PbO -based

QDs.²² However, direct structural evidence is missing. Transmission electron microscopy (TEM) cannot clearly distinguish between a PbS core and a PbCl_2 shell.^{14,16} This is because electron scattering techniques are dominated by the heavy lead atoms, which are present in both the PbS core and the hypothesized PbCl_x shell. Small-angle X-ray scattering (SAXS) likewise suffers from this lack of good contrast between PbS and PbCl_x . Moreover, X-ray powder diffraction (XRD) is of limited value since an epitaxial PbCl_x shell, by definition, will have the same continuous crystal structure as the PbS core.

Here, we show that small-angle neutron scattering (SANS) provides the elemental contrast needed to quantify the presence of a PbCl_x shell in oleate-capped PbCl_2 -based PbS QDs. Unlike electron and X-ray scattering probes, neutron scattering cross sections do not scale with the atomic number. SANS is well-suited to resolve all components of a colloidal nanocrystal because of significant contrast between core, surface layer, ligand–shell, and solvent resulting from different scattering length densities (SLDs) of each of these components. Additionally, the capability to shift contrast with the solvent through deuteration enhances model fitting.

Received: June 3, 2019

Accepted: June 21, 2019

Published: June 25, 2019

Our SANS analysis yields a lead chloride surface layer thickness of ~ 0.3 nm, which is consistent with a monolayer of PbCl_2 epitaxially bound to the PbS core. The difference in sizing curves is attributed to this surface layer. The ligand coverage and atomic ratios measured with SANS agree with nuclear magnetic resonance (NMR) spectroscopy and energy-dispersive X-ray spectroscopy (EDS) measurements on the same QDs. Finally, we propose an atomic surface configuration that is charge neutral and consistent with all experimental measurables.

QD Structure Determination from Neutron Scattering. In a SANS experiment, the observed intensity profile $I(q)$ for a dilute solution of centrosymmetric, monodisperse particles is related to the scattering length density (SLD) of the scattering particle as

$$I(q) = n \left(4\pi \int_0^\infty \Delta\rho(r) r^2 j_0(qr) dr \right)^2 \quad (1)$$

with n the number density of particles in solution, r the radial coordinate, $\Delta\rho(r)$ the excess SLD profile or solvent contrast, and j_0 the zeroth-order spherical Bessel function of the first kind. For a known $\rho(r)$ profile, $I(q)$ may be calculated. We propose a $\rho(r)$ profile as a linear superposition of the individual profiles of each material comprising the QD: core, surface layer, ligand, and penetrating solvent. The $\rho(r)$ profiles are calculated from a superposition of radial volume fraction profiles for each component $\varphi_i(r)$ through scaling by the bulk SLD of each material ρ_i^{bulk} . For the surface layer, the bulk SLD of stoichiometric PbCl_2 is used. Though the near-surface PbCl_x stoichiometry is unknown, this choice partitions the surface as stoichiometric PbCl_2 for the purposes of atomic ratio quantification. This is discussed later in the context of a proposed surface structure. The model we fit is inspired by the structures resulting from molecular dynamics (MD) simulations, and we leverage a Markov chain Monte Carlo (MCMC) fitting procedure within the framework of Bayesian inference to determine statistically robust structural parameters.²³ The MD results and fitting procedure are described in the [Supporting Information](#). When performing the fit, a ligand consistency constraint is implemented such that the number of oleate ligand head groups near the surface is equal to the number of full ligand molecules as measured by integrating the ligand volume fraction profile. The head and tail of the ligand are accounted separately because the carboxylate head has a different SLD than the aliphatic tail.

SANS data for 3 separate batches of PbS QDs were collected at 9 deuteration fractions each, ranging from 17.8% to 100% deuteration, yielding 27 independent $I(q)$ scattering curves. All 3 batches of QDs were synthesized according to the Weidman et al. method,¹⁴ using PbCl_2 and elemental sulfur in oleylamine as the reactants with a Pb/S ratio of 24:1. Nominal core sizes and polydispersities for each batch as measured by UV–vis spectroscopy are 6.2 ($\sigma_d \leq 4.1\%$), 6.8 ($\sigma_d \leq 4.4\%$), and 7.7 nm ($\sigma_d \leq 4.2\%$).¹⁴ [Figure 1a](#) shows the fit of the SLD profile to the experimental data using the MD-inspired composite model. Only a subset of the intensity profiles are shown for clarity. The full fits for all batches are shown in the [Supporting Information](#). The corresponding $\varphi(r)$ and $\rho(r)$ profiles are shown in [Figure 1b](#) and [1c](#), respectively. Multiple parameter sets sampled from the fit parameter distributions are plotted as transparencies to visually demonstrate the uncertainty of the

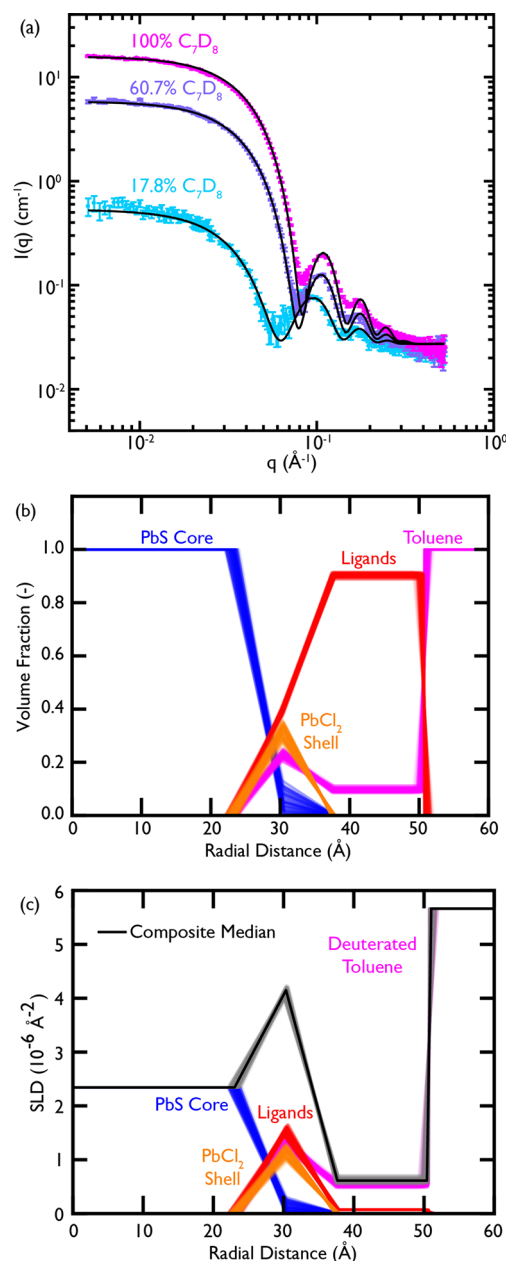


Figure 1. SANS data fitting. (a) Fit intensity profiles of 3 selected deuteration fractions chosen for clarity. (b) Fit volume fraction profile. (c) Fit scattering length density (SLD) profile for the fully deuterated sample. 100 transparent parameter set samples are plotted for each series, demonstrating the credible region.

fit. Correlations between parameters are minimal and are discussed in the [Supporting Information](#).

Our structural model predicts the intensity profiles well over the full q range and across all solvent deuteration fractions ([Figures 1](#) and [S6](#)). The shift in the first scattering peak near 0.1 \AA^{-1} with changing solvent deuteration fraction arises from solvent penetration into the ligand shell, which is captured in our structural model shown in [Figure 1b](#). The SLD profile for one of the 27 core size/deuteration combinations is shown in [Figure 1c](#). Ligand carboxylate head groups and the proposed PbCl_2 shell both have higher SLDs than PbS , leading to a peak in the composite SLD profile near the PbS surface (black curve, [Figure 1c](#)). The ligand tail groups have low SLD, and so, a valley in the SLD profile is observed at higher radial

Table 1. Summary of Experimental Results^a

UV-vis (Maes et al.) ¹³	diameter (nm)	5.76	6.45	7.40
UV-vis (Weidman et al.) ¹⁴	diameter (nm)	6.22	6.83	7.66
SANS	core diameter (nm)	5.47 ^{5.60} _{5.37}	6.36 ^{6.42} _{6.29}	6.76 ^{6.86} _{6.63}
	full diameter (nm)	6.00 ^{6.05} _{5.95}	7.14 ^{7.17} _{7.10}	7.42 ^{7.47} _{7.37}
	PbCl _x thickness (nm)	0.26 ^{0.29} _{0.22}	0.39 ^{0.41} _{0.37}	0.33 ^{0.37} _{0.29}
qNMR	lig. per QD	544 ± 66	916 ± 31	1009 ± 6
SANS	lig. per QD	719 ⁷²⁶ ₇₁₁	748 ⁷⁵² ₇₄₃	923 ⁹²⁸ ₉₁₃
	lig. cov. (nm ⁻²)	5.87 ^{5.95} _{5.75}	4.30 ^{4.35} _{4.26}	4.91 ^{4.98} _{4.81}
EDS	Pb (%)	41.4 ± 1.5	42.3 ± 1.4	44.2 ± 1.0
	S (%)	35.6 ± 8.6	38.7 ± 8.6	36.5 ± 5.6
	Cl (%)	23.0 ± 7.0	19.0 ± 5.9	19.3 ± 3.7
	total Pb:S	1.16 ± 0.28	1.09 ± 0.24	1.21 ± 0.19
SANS	Pb (%)	50.2 ^{50.6} _{49.8}	47.7 ^{47.9} _{47.5}	48.8 ^{49.1} _{48.4}
	S (%)	33.8 ^{35.6} _{32.4}	32.9 ^{33.6} _{32.1}	35.0 ^{36.3} _{33.7}
	Cl (%)	16.1 ^{17.5} _{13.6}	19.3 ^{20.4} _{18.3}	16.2 ^{17.9} _{14.4}
	core Pb:S	1.25 ^{1.26} _{1.23}	1.16 ^{1.16} _{1.15}	1.16 ^{1.17} _{1.15}
	total Pb:S	1.48 ^{1.53} _{1.42}	1.43 ^{1.48} _{1.42}	1.39 ^{1.44} _{1.35}

^aValues determined from small-angle neutron scattering (SANS) represent the median of the computed descriptors from 100 samples of the posterior. Bounds denote the extents of the central 95% credible region. Values determined from nuclear magnetic resonance (NMR) and energy-dispersive X-ray spectroscopy (EDS) denote the mean of repeat measurements with the propagated uncertainty interval from the measurement.

positions. Solvent penetration into the shell modulates the SLD profile, leading to a substantial radial variation in the SLD outside the PbS core as the deuteration fraction is changed (Figure S6b, f, and j); this variation allows for unique characterization of the solvent penetration into the ligand shell. Because the SLD contribution of the carboxylate ligand head group is constrained by the ligand tail contribution at larger radial positions, we found that varying the solvent deuteration fraction was key to separately parsing the contributions of PbCl₂ and carboxylate head groups to the SLD peak at the PbS surface. The high ligand volume fraction in the shell is consistent with the high ligand coverage samples from MD simulation shown in Figure S4.

Importantly, when we fit our model to SANS data for PbS QDs prepared from a PbO precursor, the fitted volume fraction of the PbCl₂ surface layer was identically zero (Figure S7). Moreover, if we fit our PbCl₂-derived PbS QD SANS data to a model that does not allow for any presence of PbCl₂, then the fit returns a ligand coverage that is unfeasibly large and inconsistent with NMR measurements. These observations underscore the uniqueness of the SANS fit and strongly support the PbCl_x surface layer conclusion.

Quantification of the Atomic Composition. The fit $\varphi(r)$ profiles may be used to quantify each component of the colloidal QD. These profiles correspond to a mass density profile when scaled by the bulk mass density. The mass density profiles may be integrated to obtain the total mass of each material by

$$m_i = \int_V \rho(r) dV = \int_0^\infty 4\pi r^2 \rho_i^{\text{bulk}} \varphi_i(r) dr \quad (2)$$

with m_i the mass of each material, $\rho(r)$ the mass density profile, ρ_i^{bulk} the bulk density of material i , and $\varphi_i(r)$ the fit volume fraction profile of each material. The mass can be converted to a number of molecules using the molecular weight. We then

use the number of PbS, PbCl₂, and ligand molecules to count the number of atoms and calculate atomic ratios. Because we chose the SLD of bulk PbCl₂ for scaling the volume fraction profile, the number of molecules calculated are stoichiometric

$$N_{\text{Pb,shell}} = N_{\text{PbCl}_2} \quad (3)$$

$$N_{\text{Cl,shell}} = 2N_{\text{PbCl}_2} \quad (4)$$

In a stoichiometric PbS core, the sum of the number of Pb and S atoms is twice the number of PbS pairs: $N_{\text{Pb,core}} + N_{\text{S,core}} = 2N_{\text{PbS}}$. However, the PbS core is not stoichiometric and $N_{\text{Pb,core}}$ will be greater than $N_{\text{S,core}}$. This ratio of lead to sulfur is calculated from a charge balance with the ligands, assuming each ligand and excess lead atom provide a 1- charge and 2+ charge, respectively. The combined mass and charge balances yield

$$N_{\text{Pb,core}} = N_{\text{PbS}} + \frac{N_{\text{ligand}}}{4} \quad (5)$$

$$N_{\text{S,core}} = N_{\text{PbS}} - \frac{N_{\text{ligand}}}{4} \quad (6)$$

In addition to the number of atoms and atomic ratios, the mass of PbS and PbCl₂ may be used to calculate an equivalent core diameter, PbCl₂ shell thickness, and total nanocrystal diameter including the PbCl₂ shell. The number of ligand molecules is divided by the surface area based on total core diameter to obtain a ligand coverage. In this calculation, the surface area is divided by 0.9212, the maximal sphericity of a truncated octahedron family QD, as the actual surface area is larger than that of a sphere.

Table 1 summarizes our complete SANS characterization and also includes external measurements of the core size by UV-vis spectroscopy,^{13,14} number of ligands from quantitative nuclear magnetic resonance spectroscopy (qNMR),²⁴ and

elemental ratios determined by energy-dispersive X-ray spectroscopy (EDS). The values given from SANS represent the median of these computed descriptors for 100 samples from the parameter distributions, as well as the central 95% credible region. For qNMR and EDS, the values quoted are the mean of repeat measurements with propagated uncertainty based on the standard deviation.

The measured PbCl_x shell thickness (~ 0.3 nm, Table 1) is commensurate with a monolayer coverage of PbCl_2 on the PbS surface. Previous experimental work studied the structure of PbCl_2 growth on PbS and showed that PbCl_2 can grow epitaxially on PbS with minimal lattice distortion.^{17,25} The structure of this PbCl_x shell is discussed further in the following section.

The nominal sizes predicted by the Weidman sizing curve (large excess PbCl_2) are significantly larger than the PbS core sizes extracted from SANS analysis, but close to the total nanocrystal diameter as measured by SANS (Table 1). The Weidman calibration curve was constructed from a combination of SAXS and TEM measurements, and likely reflects the total diameter of the nanocrystal (both PbS core and PbCl_x shell). However, the SANS PbS core diameter is close to that predicted by the sizing curves of Moreels et al. (PbCl_2 -based, low excess PbCl_2) and Maes et al. (PbO -based), which used TEM and SAXS, respectively, to quantify core size (Figure 2).^{13,26} Deviations of the SANS measurements from the sizing

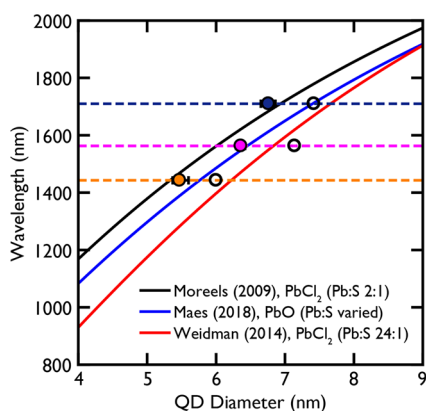


Figure 2. Comparison of UV-vis sizing curves with SANS results. SANS PbS-core-only (filled circles) and total diameter (open circles) are plotted alongside three published sizing curves.^{13,14,26} Error bars are the 95% credible region. Error bars smaller than the size of the marker are not shown.

curves are minimal and likely stem from the discretization of the core surface in the model. These comparisons are consistent with SANS measurements on PbO-derived PbS QDs and suggest that neither the PbO route nor the PbCl_2 route with low excess PbCl_2 lead to a measurable PbCl_x shell.¹⁶

Ligand coverage agrees well with previous experimental measurements on PbS and PbSe in the range of 3–5 nm⁻².^{27–29} Although the ligand coverage of the smallest QDs measured is high, it does not exceed the maximum based on charge balance with excess lead atoms for a representative octahedral core shape. When compared to the values measured by qNMR, the SANS results are both higher and lower across the three batches with an average relative error of 21%. The qNMR results assume accurate knowledge of the concentration or number density of QDs in solution, which incurs more error than is accounted for in the repeat

measurement uncertainty quoted. However, the SANS-based ligand coverages are estimated in a self-consistent way with the core size, without assuming knowledge of the concentration.

The core Pb/S ratio matches the range of 1.1–1.3 expected for the truncated octahedron family in this size range.³⁰ The total Pb/S ratio estimated by SANS accounting for the PbCl_x surface supports elevated values measured by Weidman et al. using EDS on batches made from the same synthesis.¹⁴ Though the total Pb/S ratio measured by EDS for the QDs in this study is lower than estimated by SANS, there are wide uncertainty margins on the sulfur and chlorine elemental ratios due to difficulty identifying those materials in the EDS measurement. SANS does not have the same difficulty because of the high SLD of PbCl_2 . Despite the uncertainty in the EDS measurement, the reported chlorine percentages from both techniques are in agreement.

Although batches of PbCl_2 -derived QDs are known to evolve shortly after synthesis as PbCl_2 precipitates out of solution,^{12,14,16,26} this is not a confounding variable in this study. Additional elemental quantification shows one month is sufficient for any precipitation to occur. Inductively coupled plasma optical emission spectrometry (ICP-OES) and mass spectrometry (ICP-MS) were used to measure atomic ratios on a comparable batch of QDs one month after synthesis. The measured atomic percentages were $45.6 \pm 4\%$ lead, $34.8 \pm 4\%$ sulfur, and $19.6 \pm 4\%$ chlorine. The Pb/S ratio was 1.31 ± 0.19 . This chlorine population matches that of the QDs measured with SANS, which was performed over a year after synthesis. These results suggest most of the PbCl_2 that will precipitate out of solution after synthesis does so within one month as the measured chlorine percentages are the same one month or one year after synthesis. Following this first month, we observe a negligible blue shift (less than 5 nm change in peak position) between one month and one year after synthesis.

Proposed PbCl_x Surface Layer Structure. We complete our near-atomistic characterization with a description of the core shape and surface PbCl_x structure. The core Pb/S ratio can be used with the equivalent volume diameter to map the experimental batches to a model core. Octahedra, truncated octahedra, and cuboctahedra have, respectively, lower Pb/S ratios as the shapes increasingly resemble the bulk cubic structure. For each individual shape, the ratio also decreases as the core size increases. There is a unique combination of atomic ratio to size for each batch. Figure 3 shows these approximate ideal models for each of the 3 batches measured. As the QDs grow in size, the (100) stoichiometric facets become larger. The models resemble the growth pathway previously observed.³⁰ The model cores used for MD simulation correspond well with the extracted model cores, and the surfaces of these models are used for further consideration of the PbCl_x shell structure.

We propose that the PbCl_x shell is a near-monolayer of epitaxially bound, near-stoichiometric PbCl_2 on both (100) and (111) facets of the QDs (Figure 4). It has been observed previously that PbCl_2 can grow on the (100) facets of PbS with minimal lattice strain,²⁵ and halides have been introduced post-synthesis to protect the exposed (100) facets from surface oxidation.¹⁷ Epitaxial growth is consistent with our observation that no separate crystalline PbCl_2 peaks are observed in the X-ray diffraction (XRD) pattern after full precipitation of excess PbCl_2 .¹⁴ However, the number of chlorine atoms we measure is too high to be solely bound to the (100) facets without

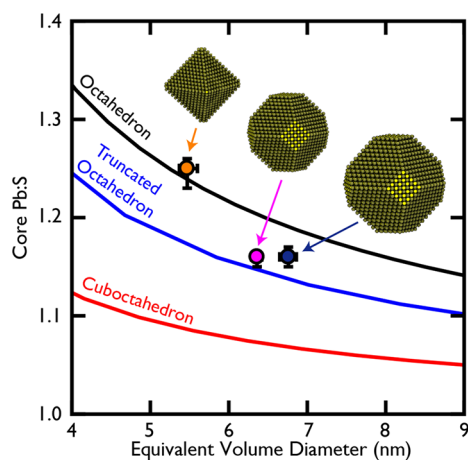


Figure 3. Shape dependence of the Pb/S ratio. The core Pb/S ratio as a function of size for different core models in the phase space for regular octahedra (black), truncated octahedra (blue), and cuboctahedra (red).

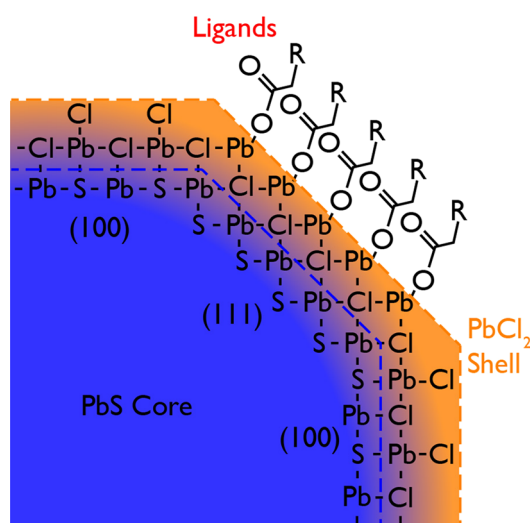


Figure 4. Proposed structure of the PbCl_x shell. A pristine PbS core (blue) is covered in a monolayer of PbCl_2 (orange) over both (100) and (111) facets. The three-dimensional structure, including oleate ligand bound to the (111) facets, is charge neutral.

multiple layers. Moreover, the smallest batch of QDs measured is nearly octahedral in shape with minimal exposed (100) surface area—yet this batch still has a comparable chlorine fraction to the others measured. Even for lower Pb/S ratios with more exposed (100) surface area, reasonable core shapes would not present enough binding sites for a monolayer of PbCl_2 with the appropriate number of chlorine atoms. Consequently, we conclude that there must be PbCl_2 bound to the (111) facets as well.

Strain within the PbCl_x layer on the (111) facet may be the reason that growth of the PbCl_x shell is limited to one monolayer. When comparing sizing curves in Figure 2, the difference between the Maes et al. and Weidman et al. curves decreases for larger core sizes. This matches the expected trend for a constant-thickness PbCl_x layer, regardless of the core diameter. Additionally, most of the chloride ions are bound to the (111) facets in this described framework, which reduce in fraction of total surface area as the core size increases.

We also consider ligand binding to the surface layer. Full surface termination in chloride ions would not present any Pb binding sites for the oleate ligands. Likewise, there are not enough lead atoms in the measured PbCl_2 layer to provide full coverage of a Pb-terminated (111) facet on top of a chloride monolayer presenting outwardly for ligand binding. A proposed schematic with Pb-oleate binding on the (111) facets is presented in Figure 4.

The (100) facets are terminated in PbCl_2 “molecules” similar to the proposed PbX_2 adlayer by Woo et al.¹⁷ On the (111) facets, a monolayer of chlorine atoms occupies the lattice sites where an additional layer of sulfur would be present if the QD grew larger. These chlorides ions are bound to lead atoms terminating the (111) facets which form the binding sites for oleate ligands. This description means the approximate core models in Figure 3 use a slightly elevated Pb/S ratio as some of the lead atoms attributed to the PbS core must terminate the PbCl_2 layer. Thus, the exact cores might resemble truncated octahedra or cuboctahedra for larger sizes. Despite this precise positioning of individual atoms being beyond the capability of this measurement, the core ratio should still be reasonably accurate as it was derived from a charge balance with the ligands. As such, the proposed models are still accurate as descriptors for the core shape. Importantly, the proposed surface structure shown in Figure 4 is charge neutral and consistent with the dimensions and mass fractions obtained from SANS.

In summary, in this work we have leveraged SANS to quantify the PbCl_2 surface on PbS QDs. This study reconciles differences in reported sizing curves for PbS QDs prepared from different PbO or PbCl_2 precursors with varying excess PbCl_2 ratios. The implications of using a particular synthesis for an application must be considered. PbO-based QDs are ideal for charge transport applications because there is no insulating surface layer, yet these materials are susceptible to surface oxidation. PbCl_2 -based QDs synthesized from a high excess PbCl_2 ratio are well-suited to self-assembly, structural studies, and luminescence applications because of their long-term colloidal stability and excellent monodispersity.

EXPERIMENTAL SECTION

Synthesis. PbCl_2 -derived PbS quantum dots were synthesized according to a previously published hot-injection method with PbCl_2 (Alfa Aesar, 99.999%) and elemental S (Sigma-Aldrich, $\geq 99.99\%$) in oleylamine (Sigma-Aldrich, $\geq 98\%$ primary amine) as the precursors.¹⁴ A Pb/S ratio of 24:1 was used. Oleic acid (Sigma-Aldrich, 90%) was used for initial crashout and ligand exchange. Methanol (Sigma-Aldrich, $\geq 99.8\%$) and ethanol (KOPTEC, anhydrous 100%) were used for additional crashouts followed by redispersion in hexanes (ACS, $\geq 98.5\%$).

An additional batch of PbO-derived PbS quantum dots were synthesized using a modification of the hot-injection protocols from Hines & Scholes and Colbert et al.^{11,31} PbO (450 mg (2.0 mmol), Sigma-Aldrich, $\geq 99\%$), 14 g of 1-octadecene (Sigma-Aldrich, 90%), and 1.4 g (4.96 mmol) of oleic acid (Sigma-Aldrich, 90%) were used for the lead precursor. The mixture was stirred under vacuum at 120 °C for 3 h, turning the solution clear. The flask was placed under flowing nitrogen gas, and the temperature was raised to 130 °C. Meanwhile, the sulfur precursor was prepared in a second three-neck flask with 4 g of 1-octadecene and 210 μL of hexamethyldisilathiane (HMDS) (Sigma-Aldrich, synthesis grade). Following in-

jection, the heating mantle was removed after 5 seconds, and the flask was cooled by a room-temperature water bath. The QDs were isolated by precipitation with acetone followed by centrifugation. The product was then cleaned in ambient air by dissolving the precipitated QDs in ~ 3 mL of hexanes and precipitating once with acetone and twice with methanol. The precipitated QDs were then brought into the glovebox and redispersed in anhydrous toluene.

UV–vis Spectrophotometry. Absorption spectra were measured using a Cary 5000 UV–vis–NIR spectrophotometer. For measurement, the QDs were suspended in tetrachloroethylene. The core diameters (dispersity σ_d) for the PbCl_2 -derived PbS QDs were measured to be 6.22 ($\sigma_d \leq 4.1\%$), 6.83 ($\sigma_d \leq 4.4\%$), and 7.66 nm ($\sigma_d \leq 4.2\%$).¹⁴ For the PbO-based QDs, the core size using the Maes et al. sizing curve was found to be 3.41 nm ($\sigma_d \leq 4.5\%$).¹³

SANS Sample Preparation. SANS samples were prepared by evaporating off the hexanes solvent overnight in a vacuum chamber before redispersion in a measured mixture of hydrogen-bearing (ACS, $\geq 99.5\%$) and deuterated toluene (Sigma-Aldrich, $\geq 99.6\%$ C_7D_8) to an approximate total scatterer volume fraction of 1.0 v/v%. A ligand coverage of 3 ligands/nm² was assumed for this calculation. The true volume fraction is fit from the data. For each batch of QDs, 9 different deuteration fractions were used ranging from 17.8% to 100%.

SANS Instrument and Data Reduction. SANS experiments were performed on the NG7-SANS instrument at the NIST Center for Neutron Research (NCNR).³² Three detector distances were used to cover the q range from approximately 0.004 \AA^{-1} to about 0.55 \AA^{-1} . The neutron wavelength for all detector configurations was 6 \AA with the wavelength spread of 12%. The samples were loaded into demountable titanium cells with quartz windows provided by NCNR. The obtained data were reduced using the SANS data reduction package of NCNR.³³

Proton Nuclear Magnetic Resonance Spectroscopy. ¹H-NMR was performed on a three-channel Bruker Avance Neo spectrometer operating at 500.34 MHz equipped with a 5 mm liquid-nitrogen cooled Prodigy broad band observe (BBO) cryoprobe. The instrument runs in full-automation off of a SampleXpress 60 sample charger. Known quantities of QDs, measured by absorbance,²⁶ were dissolved in 650 μL of deuterated toluene containing a known quantity (2 μL) of dibromomethane as an internal quantitative standard. Measurement temperature was 25 $^\circ\text{C}$. The spectra were measured under conditions of full T_1 relaxation (delay of 45 s). The integrated area under the CH_2Br_2 resonance (3.98 ppm) and the bound ligand vinyl proton resonance (5.71 ppm) were used to measure the number of ligands per QD. The vinyl proton resonance of bound ligands is shifted downfield and broadened from that of free ligands (5.49 ppm), so free and bound ligand populations can be separately quantified.²⁷ Figure S1 demonstrates that the standard and ligand peaks are well separated from solvent.

Energy Dispersive X-ray Spectroscopy. EDS was conducted on a JEOL JEM 2010FEG Transmission Electron Microscope operating at 200 kV, equipped with an Oxford INCA EDS system. A range of 5–9 measurements were performed for each batch of QDs.

Inductively Coupled Plasma Spectroscopy. Inductively coupled plasma–optical emission spectrometry (ICP-OES) and mass spectrometry (ICP-MS) were performed on a comparable batch of QDs to the three measured by SANS.

ICP-OES was used to quantify the lead and sulfur weight percentages. ICP-MS was used to supplement this measurement for chlorine weight percentage as ICP-OES cannot accurately measure the chlorine fraction.

For ICP-OES, a Perkin Elmer Optima 7300 V instrument was used with WinLab32 ICP, version 5.1.3.0550, software. Solution samples were aspirated and converted to an aerosol through a nebulizer (Teflon GemCone) in a spray chamber (Cyclonic) and directed into an argon plasma. Here, the sample was dried, vaporized, atomized, and ionized in the argon plasma, which generated emission spectra. The resulting light emissions were then directed through a series of lenses, where the emitted light was focused onto a detector, measuring the wavelengths characteristic of the elements present. The constituents of an unknown sample could then be identified and quantified. Three replicates were prepared using 50 mg of sample each. The acid digestion media consisted of a combination of trace metals grade nitric acid, hydrogen peroxide, and 18.2 M Ω deionized water. All elements analyzed were calibrated with a minimum calibration coefficient of 0.996. Quality control standards were run at the start and finish of the run with a minimum acceptance criterion of $\pm 15\%$. Typical uncertainties range from 3% to 5% at the 95% confidence level.

For ICP-MS, a Nexion 350D instrument was used with a Cetac ASX-520 auto sampler. Solution samples were aspirated and converted to an aerosol through a nebulizer (Opalmist) in a spray chamber (Tracey PFA44) and directed into an argon based plasma. Here, the sample was dried, vaporized, atomized, and ionized in the argon plasma. The resulting ions were then directed into a quadrupole mass analyzer where they were then separated and measured according to their mass to charge ratios. Five replicates were performed.

■ COMPUTATIONAL METHODS

Molecular Dynamics Simulations. PbS nanocrystals are faceted in shape with exposed {100} and {111} crystal planes. By specifying the number of atoms along any adjoining planes, we generated core models in the typical truncation sequence from octahedron, through truncated octahedron, to cuboctahedron. Ligands were grafted exclusively onto (111) facets in line with computational and experimental results.^{28,34} Coverage was manually varied as ligand coverage is known to vary in experiment. Electrostatic interactions were excluded from the simulations. The core was prescribed as a rigid body and ligands were bound to individual lead atoms such that no surface rearrangement was allowed; the simulation was purely to probe potential core, surface, and ligand-shell shapes. We used an explicit toluene solvent. Simulation parameters and methodology were the same as reported in Winslow et al.²³ The simulation results were used to generate profiles of the radial volume fraction distribution of each material from the nanocrystal center. A bin width of 4 \AA was used for these histograms.

■ ASSOCIATED CONTENT

Supporting Information

The following files are available free of charge. The Supporting Information is available free of charge on the ACS Publications website at DOI: 10.1021/acsmaterialslett.9b00200.

NMR spectra for ligand quantitation, SANS intensity curves and data analysis methodology, additional core

shape MD volume fraction profiles, corner plot for the fit parameters to the data shown in the main text, and full fits to SANS data for PbCl₂- and PbO-based QDs (PDF)

Spreadsheet of background-corrected SANS data, including *q* resolution and scattering intensity, at nine deuteration fractions for the nominally 6.2 nm batch (CSV)

Spreadsheet of background-corrected SANS data, including *q* resolution and scattering intensity, at nine deuteration fractions for the nominally 6.3 nm batch (CSV)

Spreadsheet of background-corrected SANS data, including *q* resolution and scattering intensity, at nine deuteration fractions for the nominally 7.7 nm batch (CSV)

AUTHOR INFORMATION

Corresponding Authors

*E-mail: jswan@mit.edu.

*E-mail: tisdale@mit.edu.

ORCID

Samuel W. Winslow: 0000-0003-2756-4132

Yun Liu: 0000-0002-0944-3153

William A. Tisdale: 0000-0002-6615-5342

Notes

Certain commercial equipment, instruments, or materials are identified in this document. Such identification does not imply recommendation or endorsement by the National Institute of Standards and Technology nor does it imply that the products identified are necessarily the best available for the purpose. The authors declare no competing financial interest.

ACKNOWLEDGMENTS

The authors thank Brad Olsen for helpful conversations in interpreting SANS data and Yong Zhang for assistance in performing EDS measurements. The authors also thank Mark Wilson and Philippe Green for first pointing out the sizing curve discrepancy and suggesting the presence of a PbCl_x shell. Y.L. acknowledges support by the Center for High Resolution Neutron Scattering (CHRNS), a partnership between the National Institute of Standards and Technology and the National Science Foundation under Agreement No. DMR-1508249. J.W.S. was supported by the MIT Portugal Seed Fund. W.A.T. was supported by the Camille and Henry Dreyfus Foundation.

REFERENCES

- (1) Kagan, C. R.; Lifshitz, E.; Sargent, E. H.; Talapin, D. V. Building devices from colloidal quantum dots. *Science* **2016**, *353*, aac5523.
- (2) Alivisatos, A. P. Semiconductor clusters, nanocrystals, and quantum dots. *Science* **1996**, *271*, 933–937.
- (3) Nozik, A. J. Quantum Dot Solar Cells. *Phys. E* **2002**, *14*, 115–120.
- (4) Konstantatos, G.; Howard, I.; Fischer, A.; Hoogland, S.; Clifford, J.; Klem, E.; Levina, L.; Sargent, E. H. Ultrasensitive solution-cast quantum dot photodetectors. *Nature* **2006**, *442*, 180–183.
- (5) Koleilat, G. I.; Levina, L.; Shukla, H.; Myrskog, S. H.; Hinds, S.; Pattantyus-Abraham, A. G.; Sargent, E. H. Efficient, Stable Infrared Photovoltaics Based on Solution-Cast Colloidal Quantum Dots. *ACS Nano* **2008**, *2*, 833–840.
- (6) Choi, J. J.; Lim, Y. F.; Santiago-Berrios, M. B.; Oh, M.; Hyun, B.-R.; Sun, L.; Bartnik, A. C.; Goedhart, A.; Malliaras, G. G.; Abruña, H.

D.; et al. PbSe Nanocrystal Excitonic Solar Cells. *Nano Lett.* **2009**, *9*, 3749–3755.

(7) Talapin, D. V.; Lee, J.-S.; Kovalenko, M. V.; Shevchenko, E. V. Prospects of Colloidal Nanocrystals for Electronic and Optoelectronic Applications. *Chem. Rev.* **2010**, *110*, 389–458.

(8) Brown, P. R.; Kim, D.; Lunt, R. R.; Zhao, N.; Bawendi, M. G.; Grossman, J. C.; Bulović, V. Energy Level Modification in Lead Sulfide Quantum Dot Thin Films through Ligand Exchange. *ACS Nano* **2014**, *8*, 5863–5872.

(9) Bozyigit, D.; Yazdani, N.; Yarema, M.; Yarema, O.; Lin, W. M. M.; Volk, S.; Vuttivorakulchai, K.; Luisier, M.; Juranyi, F.; Wood, V. Soft surfaces of nanomaterials enable strong phonon interactions. *Nature* **2016**, *531*, 618–622.

(10) Yazdani, N.; Bozyigit, D.; Vuttivorakulchai, K.; Luisier, M.; Infante, I.; Wood, V. Tuning Electron-Phonon Interactions in Nanocrystals through Surface Termination. *Nano Lett.* **2018**, *18*, 2233–2242.

(11) Hines, M. A.; Scholes, G. D. Colloidal PbS Nanocrystals with Size-Tunable Near-Infrared Emission: Observation of Post-Synthesis Self-Narrowing of the Particle Size Distribution. *Adv. Mater.* **2003**, *15*, 1844–1849.

(12) Cademartiri, L.; Bertolotti, J.; Sapienza, R.; Wiersma, D. S.; von Freymann, G.; Ozin, G. A. Multigram Scale, Solventless, and Diffusion-Controlled Route to Highly Monodisperse PbS Nanocrystals. *J. Phys. Chem. B* **2006**, *110*, 671–673.

(13) Maes, J.; Castro, N.; De Nolf, K.; Walravens, W.; Abécassis, B.; Hens, Z. Size and Concentration Determination of Colloidal Nanocrystals by Small-Angle X-Ray Scattering. *Chem. Mater.* **2018**, *30*, 3952–3962.

(14) Weidman, M. C.; Beck, M. E.; Hoffman, R. S.; Prins, F.; Tisdale, W. A. Monodisperse, Air-Stable PbS Nanocrystals via Precursor Stoichiometry Control. *ACS Nano* **2014**, *8*, 6363–6371.

(15) Moreels, I.; Justo, Y.; De Geyter, B.; Hastraete, K.; Martins, J. C.; Hens, Z. Size-Tunable, Bright, and Stable PbS Quantum Dots: A Surface Chemistry Study. *ACS Nano* **2011**, *5*, 2004–2012.

(16) Brittan, S.; Colbert, A. E.; Brintlinger, T. H.; Cunningham, P. D.; Stewart, M. H.; Heuer, W. B.; Stroud, R. M.; Tischler, J. G.; Boecker, J. E. Effects of a Lead Chloride Shell on Lead Sulfide Quantum Dots. *J. Phys. Chem. Lett.* **2019**, *10*, 1914–1918.

(17) Woo, J. Y.; Ko, J. H.; Song, J. H.; Kim, K.; Choi, H.; Kim, Y. H.; Lee, D. C.; Jeong, S. Ultrastable PbSe nanocrystal quantum dots via in situ formation of atomically thin halide adlayers on PbSe(100). *J. Am. Chem. Soc.* **2014**, *136*, 8883–8886.

(18) Liu, Y.; Gibbs, M.; Puthussery, J.; Gaik, S.; Ihly, R.; Hillhouse, H. W.; Law, M. Dependence of carrier mobility on nanocrystal size and ligand length in pbse nanocrystal solids. *Nano Lett.* **2010**, *10*, 1960–1969.

(19) Bozyigit, D.; Lin, W. M.; Yazdani, N.; Yarema, O.; Wood, V. A quantitative model for charge carrier transport, trapping and recombination in nanocrystal-based solar cells. *Nat. Commun.* **2015**, *6*, 6180.

(20) Gilmore, R. H.; Lee, E. M. Y.; Weidman, M. C.; Willard, A. P.; Tisdale, W. A. Charge Carrier Hopping Dynamics in Homogeneously Broadened PbS Quantum Dot Solids. *Nano Lett.* **2017**, *17*, 893–901.

(21) Gilmore, R. H.; Winslow, S. W.; Lee, E. M.; Ashner, M. N.; Yager, K. G.; Willard, A. P.; Tisdale, W. A. Inverse Temperature Dependence of Charge Carrier Hopping in Quantum Dot Solids. *ACS Nano* **2018**, *12*, 7741–7749.

(22) Nienhaus, L.; Wu, M.; Geva, N.; Shepherd, J. J.; Wilson, M. W.; Bulović, V.; Van Voorhis, T.; Baldo, M. A.; Bawendi, M. G. Speed Limit for Triplet-Exciton Transfer in Solid-State PbS Nanocrystal-Sensitized Photon Upconversion. *ACS Nano* **2017**, *11*, 7848–7857.

(23) Winslow, S. W.; Shcherbakov-Wu, W.; Liu, Y.; Tisdale, W. A.; Swan, J. W. Characterization of Colloidal Nanocrystal Surface Structure Using Small Angle Neutron Scattering and Efficient Bayesian Parameter Estimation. *J. Chem. Phys.* **2019**, *150*, 244702.

(24) Anderson, N. C.; Hendricks, M. P.; Choi, J. J.; Owen, J. S. Ligand exchange and the stoichiometry of metal chalcogenide nanocrystals: Spectroscopic observation of facile metal-carboxylate

displacement and binding. *J. Am. Chem. Soc.* **2013**, *135*, 18536–18548.

(25) Elleman, A. J.; Wilman, H. The structure and epitaxy of lead chloride deposits formed from lead sulphide and sodium chloride. *Proc. Phys. Soc., London, Sect. A* **1949**, *62*, 344–355.

(26) Moreels, I.; Lambert, K.; Smeets, D.; De Muynck, D.; Nollet, T.; Martins, J. C.; Vanhaecke, F.; Vantomme, A.; Delerue, C.; Allan, G.; et al. Size-Dependent Optical Properties of Colloidal PbS Quantum Dots. *ACS Nano* **2009**, *3*, 3023–3030.

(27) Moreels, I.; Fritzing, B.; Martins, J. C.; Hens, Z. Surface chemistry of colloidal PbSe nanocrystals. *J. Am. Chem. Soc.* **2008**, *130*, 15081–15086.

(28) Choi, J. J.; Bealing, C. R.; Bian, K.; Hughes, K. J.; Zhang, W.; Smilgies, D.-M.; Hennig, R. G.; Engstrom, J. R.; Hanrath, T. Controlling Nanocrystal Superlattice Symmetry and Shape-Anisotropic Interactions through Variable Ligand Surface Coverage. *J. Am. Chem. Soc.* **2011**, *133*, 3131–3138.

(29) Ong, W.-L.; Rupich, S. M.; Talapin, D. V.; McGaughey, A. J.; Malen, J. A. Surface chemistry mediates thermal transport in three-dimensional nanocrystal arrays. *Nat. Mater.* **2013**, *12*, 410–415.

(30) Choi, H.; Ko, J.-H.; Kim, Y.-H.; Jeong, S. Steric-Hindrance-Driven Shape Transition in PbS Quantum Dots: Understanding Size-Dependent Stability. *J. Am. Chem. Soc.* **2013**, *135*, 5278–5281.

(31) Colbert, A. E.; Wu, W.; Janke, E. M.; Ma, F.; Ginger, D. S. Effects of Ligands on Charge Generation and Recombination in Hybrid Polymer/Quantum Dot Solar Cells. *J. Phys. Chem. C* **2015**, *119*, 24733–24739.

(32) Glinka, C. J.; Barker, J. G.; Hammouda, B.; Krueger, S.; Moyer, J. J.; Orts, W. J. The 30 m Small-Angle Neutron Scattering Instruments at the National Institute of Standards and Technology. *J. Appl. Crystallogr.* **1998**, *31*, 430–445.

(33) Kline, S. R. Reduction and analysis of SANS and USANS data using IGOR Pro. *J. Appl. Crystallogr.* **2006**, *39*, 895–900.

(34) Drijvers, E.; De Roo, J.; Martins, J. C.; Infante, I.; Hens, Z. Ligand Displacement Exposes Binding Site Heterogeneity on CdSe Nanocrystal Surfaces. *Chem. Mater.* **2018**, *30*, 1178–1186.